Chapter 10

Particle Swarm Optimization of Highly Selective Digital Filters over the Finite-Precision Multiplier Coefficient Space

Seyyed Ali Hashemi and Behrouz Nowrouzian

Additional information is available at the end of the chapter

http://dx.doi.org/10.5772/52196

1. Introduction

Digital filters find wide variety of applications in modern digital signal processing systems [1, 2]. As a result of the recent progress in such systems, there is an ever growing demand for sharp transition band digital filters. These narrow transition bandwidth digital filters are usually designed by using the frequency response masking (FRM) approach [3]. The computational efficiency of the FRM technique makes it suitable for different applications, e.g. in audio signal processing and data compression [4].

Practical design of digital filters is based on optimization for satisfying the given design specifications together with the hardware architecture. However, the optimization may be carried out in terms of fixed configurations but variable multiplier coefficient values. On the other hand, the problem may concern the optimization of the hardware architecture without taking the multiplier coefficient values into consideration.

In order to optimize the given design specifications, the multiplier coefficient values can be determined in infinite precision by using hitherto optimization techniques. However, in an actual hardware implementation of the digital filters, the infinite precision multipliers should be quantized to their finite precision counterparts, but these finite precision multiplier coefficients may no longer satisfy the given design specifications. Consequently, from a hardware implementation point of view, there is a need for finite precision optimization techniques, capable of finding the optimized digital filter rapidly while keeping the computational complexity at a desired level. In principle, there exist two different techniques for the optimization of digital filters, namely, gradient-based and heuristic optimization approaches.

Gradient-based optimization techniques have been studied widely. In [5], an integer programming technique was developed for the optimization of digital filters over a discrete multiplier coefficient

space. In [6], a Remez exchange algorithm was used for the optimization of FRM finite impulse response (FIR) digital filters and it was shown that this algorithm may provide a speed advantage over the linear programming approach. However, both these techniques suffer from sub-optimality problems. In [7], unconstrained weighted least-squares criterion was used to develop another technique for the optimization of digital filters. Convex optimization approaches such as semi-definite programming [8] and second-order cone programming [9] have also been applied to the optimization of digital filters. However, if a large number of constraints are present, these optimization techniques may become computationally inefficient in terms of time consumption and speed.

Heuristic optimization algorithms have emerged as promising candidates for the design and discrete optimization of digital filters, particularly due to the fact that they are capable of automatically finding near-optimum solutions while keeping the computational complexity of the algorithm at moderate levels. Simulated annealing (SA) and genetic algorithms (GAs) were widely used in the design and optimization of digital filters [10–12]. Particle swarm optimization (PSO) and seeker optimization algorithm (SOA) are two newly developed algorithms suitable for the optimization of various digital filters due to their few number of implementation parameters and high speed of convergence [13, 14]. It was shown that SOA has advantages over PSO in terms of the speed of convergence and global search ability [15]. Tabu search (TS) [16], ant colony optimization (ACO) [17], immune algorithm (IA) [18] and differential evolution (DE) [19, 20] are alternative candidates for the optimization of digital filters. All the foregoing techniques allow a robust search of the solution space through a parallel search in all directions without any recourse to gradient information. However, the aforementioned techniques were developed for infinite precision optimization of digital filters which require the user to perform a quantization step for a hardware implementation.

In [21–23], a technique was developed for finite-precision design and optimization of FRM digital filters using GAs. finite-precision optimization of FRM FIR digital filters using PSO was studied in [24, 25] and finite-precision optimization of infinite impulse response based (IIR-based) FRM digital filters was studied in [26, 27]. PSO was originally proposed by Kennedy and Eberhart in 1995 as a new intelligent optimization algorithm which simulates the migration and aggregation of a flock of birds seeking food [28]. It adopts a strategy based on particle swarm and parallel global random search, that may exhibit superior performance to other intelligent algorithms in computational speed and memory. In PSO, a potential candidate solution is represented as a particle in a multidimensional search space, where each dimension represents a distinct optimization variable. The particles in the multidimensional search space are characterized by corresponding fitness values. They make movements in the search space towards regions characterized by high fitness values.

The conventional FRM digital filters incorporate FIR interpolation digital subfilters. These digital subfilters are usually of high orders, rendering the resulting overall FRM digital filters as not economical, since the resulting digital filters occupy large chip areas and consume high amounts of power in their VLSI hardware implementations. In general, the multiplication operation is the most cost-sensitive part in such an implementation. Therefore, there is every incentive to reduce the number of multiplication operations in the digital filter realization. This problem may be circumvented by employing IIR interpolation digital subfilters [29, 30].

There is a vast body of literature available for the design and optimization of digital IIR filters [31–33]. However, all the aforementioned designs are based on the exact transfer function coefficients which leads to an uneconomical hardware realization of such filters. In order to realize the constituent IIR interpolation digital subfilters on a hardware platform, the bilinear-lossless-discrete-integrator (bilinear-LDI) digital filter design approach is employed [34]. These digital subfilters are realized as a

http://dx.doi.org/10.5772/52196

sum/difference of a pair of bilinear-LDI digital allpass networks. The salient features of the bilinear-LDI digital filters are that they lend themselves to fast two-cycle parallel digital signal processing speeds, while being minimal in the number of digital multiplication operations (and, practically, minimal in number of digital addition and unit-delay operations).

The starting point in the design of FRM digital filters is to find the multiplier coefficients constituent in the FRM digital filter in infinite precision by using the hitherto gradient-based optimization techniques (e.g. Parks-McClellan approach [35] for FIR digital filters) followed by a quantization step. The quantization can be performed by constraining the multiplier coefficients values to conform to certain number systems such as the signed power-of-two (SPT) system. SPT is a computationally efficient number system which can further reduce the hardware complexity of the FRM IIR digital filters. In this number system, each multiplier coefficient is represented with only a few non-zero bits within its wordlength, permitting the decomposition of the multiplication operation into a finite series of shift and add operations. Digital filters incorporating SPT multiplier coefficient representation are commonly referred to as *multiplierless* digital filters [36]. However, the SPT representation of a given number is not unique, resulting in redundancy in the multiplier coefficient representation. This redundancy can adversely affect the corresponding computational complexity due to recourse to compare operations repetitively.

The canonical signed digit (CSD) number system is a special case of the SPT number system which circumvents the above redundancy problem by limiting the number of non-zero bits in the representation of the multiplier coefficients. It is usually used in combination with subexpression sharing and elimination, which in turn results in substantial reduction in the cost of the VLSI hardware implementation of the digital filters [37]. In CSD number system, no two (or more) non-zero bits can appear consecutively in the representation of the multiplier coefficients, reducing the maximum number of non-zero bits by a factor of two in terms of shift and add operations [38].

After multiplier coefficient quantization, the resulting FRM digital filter may no longer satisfy the given target design specifications. Therefore, the next step in the design of FRM digital filters is to perform a further optimization to make the finite precision FRM digital filter to conform to the design specifications. This can be achieved by resorting to a finite-precision optimization technique such as PSO.

A direct application of the conventional PSO algorithm to the optimization of the above FRM digital filters gives rise to three separate problems:

- The first problem arises because in the course of optimization, the multiplier coefficient update operations lead to values that may no longer conform to the desired CSD wordlength, etc. (due to random nature of velocity and position of particles). This problem is resolved by generating indexed look-up tables (LUTs) of permissible CSD multiplier coefficient values, and by employing the indices of LUTs to represent FRM digital filter multiplier coefficient values.
- The second problem stems from the fact that in case of FRM IIR digital filters, the resulting FRM IIR digital filters may no longer be bounded-input-bounded-output (BIBO) stable. This problem can be resolved by generation and successive augmentation of template LUTs until the BIBO stability constraints remain satisfied [23].
- Finally, the third problem arises because even in case of having indexed LUTs, the particles may go over the boundaries of LUTs in course of optimization (due to the inherent limited search space). This can be resolved by introducing *barren layers*. A barren layer is a region, with a certain width

and certain entries, which is added to the problem space such that the particles tend to shy away from such a region. The width of the barren layers is calculated based on a worst case scenario that may happen in the particles movements in the search space. However, the entries of barren layers are different for different problems and depend on the topology of the search space and the fitness function used in the problem.

This chapter discusses in detail the design, realization and discrete PSO of FRM IIR digital filters. FRM IIR digital filters are designed by FIR masking digital subfilters together with IIR interpolation digital subfilters. The FIR filter design is straightforward and can be performed by using hitherto techniques. The IIR digital subfilter design topology consists of a parallel combination of a pair of allpass networks such that its magnitude-frequency response matches that of an odd order elliptic minimum Q-factor (EMQF) transfer function. This design is realized using the bilinear-LDI approach, with multiplier coefficient values represented as finite-precision CSD numbers.

The above FRM digital filters are optimized over the discrete multiplier coefficient space, resulting in FRM digital filters which are capable of direct implementation in digital hardware platform without any need for further optimization. A new PSO algorithm is developed to tackle three different problems. In this PSO algorithm, a set of indexed LUTs of permissible CSD multiplier coefficient values is generated to ensure that in the course of optimization, the multiplier coefficient update operations constituent in the underlying PSO algorithm lead to values that are guaranteed to conform to the desired CSD wordlength, etc. In addition, a general set of constraints is derived in terms of multiplier coefficients to guarantee that the IIR bilinear-LDI interpolation digital subfilters automatically remain BIBO stable throughout the course of PSO algorithm. Moreover, by introducing barren layers, the particles are ensured to automatically remain inside the boundaries of LUTs in course of optimization.

2. The conventional PSO algorithm

Let us consider an optimization problem consisting of N design variables, and let us refer to each solution as a particle. Let us further consider a swarm of K particles in the N-dimensional search space. The position of the k-th particle in the search space can be assigned a N-dimensional position vector $X_k = \{x_{k1}, x_{k2}, \ldots, x_{kN}\}$. In this way, the element x_{kj} (for $j = 1, 2, \ldots, N$) represents the j-th coordinate of the particle X_k.

The PSO optimization fitness function maps each particle X_k in the search space to a fitness value. In addition, the particle X_k is assigned a N-dimensional velocity vector $V_k = \{v_{k1}, v_{k2}, \ldots, v_{kN}\}$. The PSO optimization search is directed towards promising regions by taking into account the velocity vector V_k together with the best previous position of the k-th particle $X_{best_k} = \{x_{best_{k1}}, x_{best_{k2}}, \ldots, x_{best_{kN}}\}$, and the best global position of the swarm $G_{best} = \{g_{best_1}, g_{best_2}, \ldots, g_{best_N}\}$ (i.e. the location of the particle with the best fitness value).

The conventional PSO is initialized by spreading the particles X_k through the search space in a random fashion. Then, the particles make movements through the search space towards regions characterized by high fitness values with corresponding velocities V_k. The movement of each particle is governed by the best previous location of the same particle X_{best_k}, and by the global best location G_{best}. The velocity of particle movement is determined from the previous best location of the particle, the global best location, and the previous velocity.

http://dx.doi.org/10.5772/52196

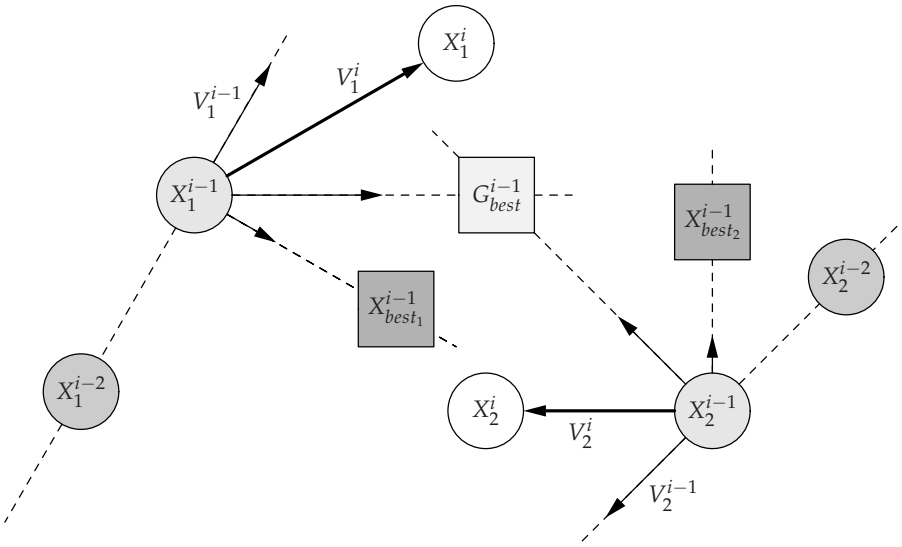

Figure 1. Movement of Particles in PSO Algorithm

The velocity and position of each particle in the i-th iteration throughout the course of PSO are updated in accordance with the equations:

$$v_{kj}^i = wv_{kj}^{i-1} + c_1 r_1 (x_{best_{kj}}^{i-1} - x_{kj}^{i-1}) + c_2 r_2 (g_{best_j}^{i-1} - x_{kj}^{i-1}) \tag{1}$$

$$\text{if} \quad v_{kj}^i < v_{min} \quad ; \quad v_{kj}^i = v_{min}$$

$$\text{if} \quad v_{kj}^i > v_{max} \quad ; \quad v_{kj}^i = v_{max}$$

$$x_{kj}^i = x_{kj}^{i-1} + v_{kj}^i \tag{2}$$

The parameter w represents an inertia weight; c_1 and c_2 are the correction (learning) factors, and r_1 and r_2 are random numbers in the interval $[0, 1]$. The velocity is limited between v_{min} and v_{max} to avoid very large particle movements in the search space, where $v_{min} < 0$ and $v_{max} > 0$. Fig. 1 illustrates how the particles move in a two-dimensional search space ($N = 2$). In this figure, two particles are present in the swarm, i.e. $K = 2$.

The first term in the right hand side of movement update Eqn. (1), weighted by w, signifies the dependence of the current particle velocity on its value in the previous iteration. The second term, weighted by c_1, signifies an attractor to pull the particle towards its previous best position. The third term, weighted by c_2 controls the movement of the particle towards the global best position.

In addition to the update Eqns. (1) and (2), one can limit the coordinates in a particle between two user defined values $x_{j_{min}}$ and $x_{j_{max}}$ in order to limit the search space. However, This operation increases the complexity and consumes time.

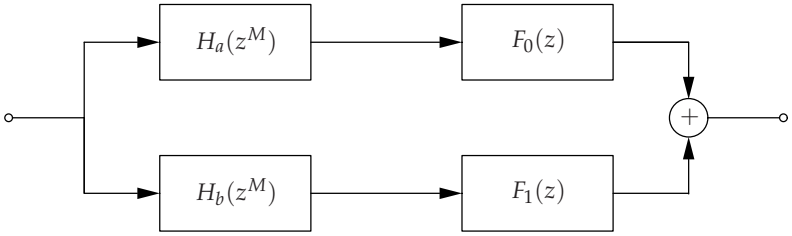

Figure 2. FRM Digital Filter Block Diagram

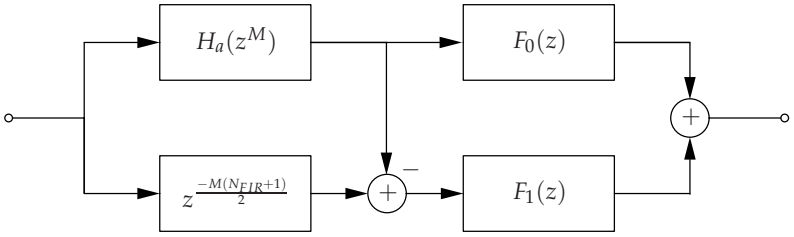

Figure 3. Block Diagram Representation of Frequency-Response Masking

3. The conventional FRM design approach

3.1. Design of lowpass FRM digital filters

The block diagram in Fig. 2 shows a conventional FRM digital filter, where $H_a(z)$ represents a FIR interpolation lowpass digital subfilter, and where $H_b(z)$ represents a power complementary counterpart of $H_a(z)$ in accordance with

$$|H_a(e^{j\omega})|^2 + |H_b(e^{j\omega})|^2 = 1 \tag{3}$$

Here, z represents the discrete-time complex frequency, and ω represents the corresponding (normalized) real frequency variable. Moreover, $F_0(z)$ and $F_1(z)$ represent FIR masking digital subfilters, while $H_a(z^M)$ and $H_b(z^M)$ represent M-fold interpolated versions of $H_a(z)$ and $H_b(z)$, respectively. In case of FIR digital interpolation subfilters, for a linear-phase filter $H_a(z)$ of order N_{FIR}, the relationship between $H_b(z)$ and $H_a(z)$ is as follows:

$$H_b(z) = z^{(N_{FIR}+1)/2} - H_a(z) \tag{4}$$

and hence $H_b(z)$ can be implemented by subtracting the output of $H_a(z)$ from the delayed version of the input, as shown in Fig. 3.

The FRM digital filter in Fig. 2 has an overall transfer function

$$H(z) = H_a(z^M)F_0(z) + H_b(z^M)F_1(z) \tag{5}$$

http://dx.doi.org/10.5772/52196

	Filter	Passband Edge	Stopband Edge
Case I	$H(z)$	$\frac{2I_L\pi+\omega_p}{M}$	$\frac{2I_L\pi+\omega_a}{M}$
	$F_0(z)$	$\frac{2I_L\pi+\omega_a}{M}$	$\frac{2(I_L+1)\pi-\omega_a}{M}$
	$F_1(z)$	$\frac{2I_L\pi-\omega_p}{M}$	$\frac{2I_L\pi+\omega_p}{M}$
Case II	$H(z)$	$\frac{2I_L\pi-\omega_a}{M}$	$\frac{2I_L\pi-\omega_p}{M}$
	$F_0(z)$	$\frac{2(I_L-1)\pi+\omega_a}{M}$	$\frac{2I_L\pi-\omega_a}{M}$
	$F_1(z)$	$\frac{2I_L\pi-\omega_p}{M}$	$\frac{2I_L\pi+\omega_p}{M}$

Table 1. Edge Frequencies of the Overall FRM FIR filter and Masking Subfilters

The masking digital subfilters $F_0(z)$ and $F_1(z)$ are employed to suppress the unwanted image bands produced by the interpolated digital subfilters $H_a(z^M)$ and $H_b(z^M)$. The masking filters are made to have equal order (by zero padding) in order to ensure that their phase characteristics are similar. The corresponding interpolated digital subfilters $H_a(z^M)$ and $H_b(z^M)$ can realize transition bands which are a factor of M sharper than those of $H_a(z)$ and $H_b(z)$, without increasing the number of required non-zero digital multipliers. The magnitude frequency-response of the various subfilters incorporated by the FRM digital filter design approach are shown in Fig. 4.

Here, Case I design is when the transition band of $H(z)$ is extracted from that of $H_a(z^M)$ and Case II design is when the transition band of $H(z)$ is extracted from that of $H_b(z^M)$. The edge frequencies of the overall digital FRM filter and its constituent subfilters are given in Table 1, where I_L represents the number of image lobes to be masked given by:

$$I_L = \begin{cases} \left\lfloor \frac{M\omega_p}{2\pi} \right\rfloor & \text{Case I} \\ \left\lceil \frac{M\omega_a}{2\pi} \right\rceil & \text{Case II} \end{cases} \tag{6}$$

where $\lfloor\ \rfloor$ denotes the largest integer from the lower side, and $\lceil\ \rceil$ signifies the smallest integer from the upper side.

3.2. Design of bandpass FRM digital filters

In general, it is possible to extend the conventional FRM approach for the design of bandpass or bandstop FRM digital filters. However, the resulting FRM digital filters are constrained to have identical lower and upper transition bandwidths. In [39], this restriction was relaxed by realizing the bandstop FRM FIR digital filter as a parallel combination of a corresponding pair of lowpass and highpass FIR

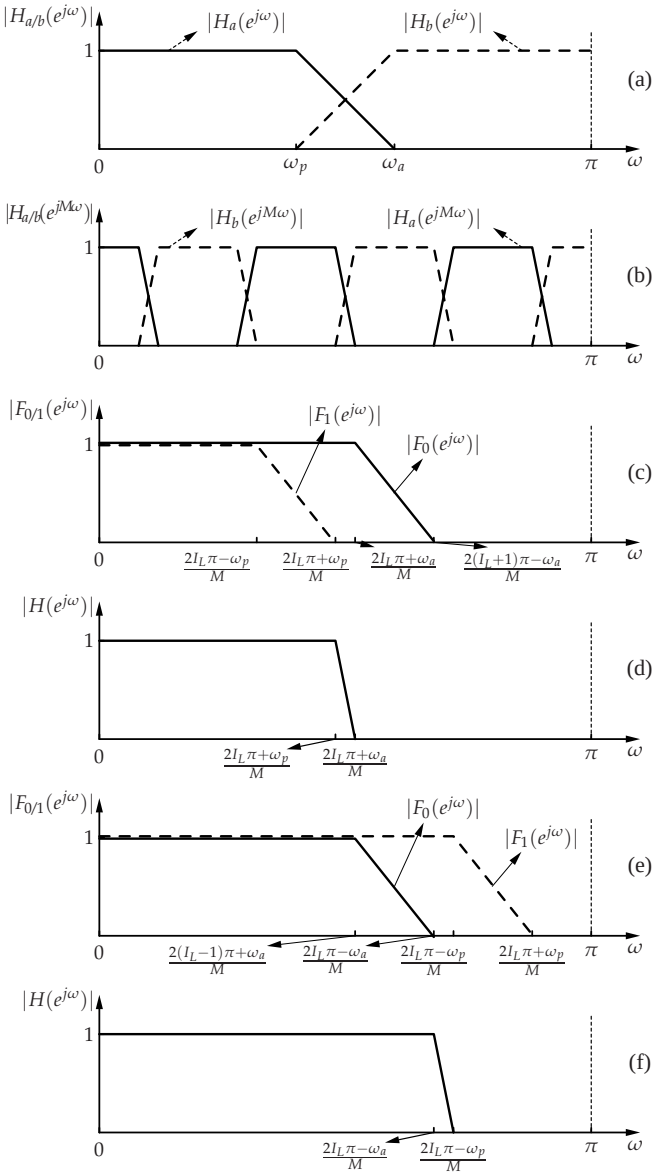

Figure 4. Magnitude Frequency-Response of FRM Digital Filter. (a) Magnitude Frequency-Response of the Bandedge-Shaping Digital Subfilters $H_a(z)$ and $H_b(z)$. (b) Magnitude Frequency-Response of the M-Interpolated Complementary Digital Subfilters $H_a(z^M)$ and $H_b(z^M)$. (c) Magnitude Frequency-Response of the Masking Digital Subfilters $F_0(z)$ and $F_1(z)$ for Case I. (d) Magnitude Frequency-Response of the Overall FRM Digital Filter $H(z)$ for Case I. (e) Magnitude Frequency-Response of the Masking Digital Subfilters $F_0(z)$ and $F_1(z)$ for Case II. (f) Magnitude Frequency-Response of the Overall FRM Digital Filter $H(z)$ for Case II [3].

http://dx.doi.org/10.5772/52196

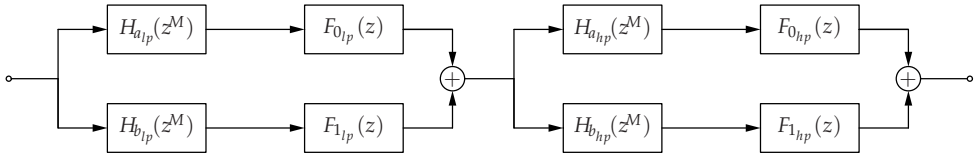

Figure 5. Bandpass FRM Digital Filter Block Diagram

digital filters. The latter lowpass and highpass FRM digital filters were obtained using a variation of the conventional FRM approach.

Let the desired bandpass FRM digital filter $H(z)$ have a lower transition bandwidth which is not identical to its upper transition bandwidth. $H(z)$ can be realized as a cascade combination of a pair of lowpass and highpass FRM digital filters, so that

$$H(z) = H_{lp}(z)H_{hp}(z) \tag{7}$$

where $H_{lp}(z)$ represents a lowpass and $H_{hp}(z)$ represents a highpass FRM digital filter. In this way, $H_{lp}(z)$ and $H_{hp}(z)$ can be obtained with the help of Eqn. (5) as

$$H_{lp}(z) = H_{a_{lp}}(z^M)F_{0_{lp}}(z) + H_{b_{lp}}(z^M)F_{1_{lp}}(z) \tag{8}$$

$$H_{hp}(z) = H_{a_{hp}}(z^M)F_{0_{hp}}(z) + H_{b_{hp}}(z^M)F_{1_{hp}}(z) \tag{9}$$

The lower transition bandwidth is governed by the constituent transition bandwidth of the highpass FRM digital filter, while the upper transition bandwidth is governed by the constituent transition bandwidth of the lowpass FRM digital filter. The realization for bandpass FRM digital filter are as shown in Fig. 5.

4. Design of FRM digital filters incorporating IIR interpolation digital subfilters

In the case of FRM IIR digital filters, $H_a(z)$ and $H_b(z)$ (in section 3) act as IIR interpolation digital subfilters. The masking filters $F_0(z)$ and $F_1(z)$ are not changed (i.e. they are still equal order FIR digital filters). Therefore, Eqn. (5) is still valid for the FRM IIR digital filter.

The IIR interpolation digital subfilter $H_a(z)$ is chosen to have an odd order N_{IIR}. Odd-ordered elliptic transfer functions can be represented as a sum of or difference between two allpass transfer functions [40]. Therefore, $H_a(z)$ can be realized as the addition of two allpass digital networks $G_0(z)$ and $G_1(z)$ as follows:

$$H_a(z) = \frac{G_0(z) + G_1(z)}{2} \tag{10}$$

where $G_0(z)$ is odd-ordered and $G_1(z)$ is even-ordered. The interesting fact is that the difference between $G_0(z)$ and $G_1(z)$ results in a filter that is power complementary to $H_a(z)$, and can subsequently be used as the power complementary interpolation digital subfilter $H_b(z)$ as in the following:

$$H_b(z) = \frac{G_0(z) - G_1(z)}{2} \tag{11}$$

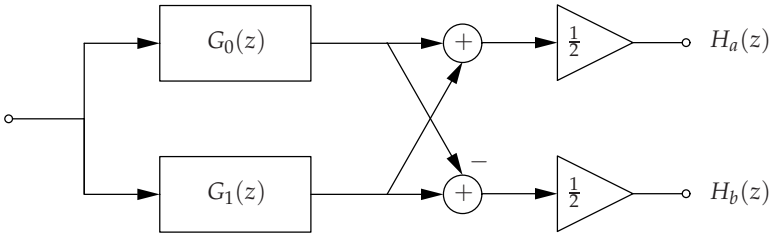

Figure 6. Block Diagram of Interpolation and Complementary Filters as a Parallel Combination of Two Allpass Networks

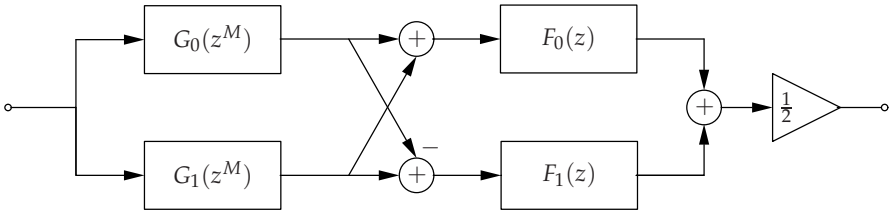

Figure 7. FRM Digital Filter Realization in Terms of Allpass Digital Networks $G_0(z)$ and $G_1(z)$

It can be easily verified that $H_a(z)$ and $H_b(z)$ are power complementary digital filters [29], i.e. they satisfy Eqn. (3). In addition, it is well known that this structure halves the number of multiplier coefficients required for the implementation of FRM digital filters and therefore is the most economical realization since it requires a total of only N_{IIR} multiplier coefficients to realize both $H_a(z)$ and $H_b(z)$. The overall transfer function of $H(z)$ given by Eqn. (5) can be expressed as:

$$H(z) = \frac{G_0(z^M) + G_1(z^M)}{2} F_0(z) + \frac{G_0(z^M) - G_1(z^M)}{2} F_1(z) \tag{12}$$

The block diagram in Fig. 6 shows the IIR interpolation digital subfilters $H_a(z)$ and $H_b(z)$ realized as a parallel combination of two allpass networks. It should be noted that if $H_a(z)$ is a lowpass filter, $H_b(z)$, which is the power complementary of $H_a(z)$, is a highpass filter. Fig. 7 shows an overall FRM IIR digital filter realization.

One may rearrange the structure in Fig. 7 by using Eqns. (10-11). This can be performed by defining two digital subfilters as follows:

$$A(z) = \frac{F_0(z) + F_1(z)}{2} \tag{13}$$

$$B(z) = \frac{F_0(z) - F_1(z)}{2} \tag{14}$$

Then $H(z)$ in Eqn. (12) simplifies to:

$$H(z) = G_0(z^M)A(z) + G_1(z^M)B(z) \tag{15}$$

http://dx.doi.org/10.5772/52196

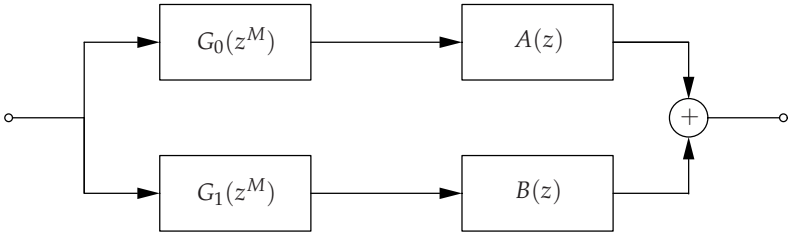

Figure 8. Alternative Structure of the Overall FRM IIR Digital Filter

Fig. 8 shows the block diagram representing Eqn. (15).

The advantage of realizing the FRM IIR digital filter as shown in Fig. 8 is that two adders shown in Fig. 7 are removed and they are no longer required. This subsequently simplifies the hardware implementation of the overall FRM IIR digital filter. However, it should be noted that the FIR masking digital subfilters $F_0(z)$ and $F_1(z)$ are made to be equal order using zero padding, and this results in the masking filters being moderately sparse. This is not the case when $A(z)$ and $B(z)$ are used instead. Therefore, the gain in hardware that could be achieved by using the realization in Fig. 8 is offset by a greater number of non-zero multiplier coefficients required in the realization of FRM IIR digital filters.

5. Realization of IIR interpolation digital subfilters using Elliptic Filters with Minimum Q-factor (EMQF)

Bilinear-LDI transformation falls into the category of digital filter realization techniques that transform an analog reference filter to its digital counterpart. Therefore, in order to determine the multiplier coefficient values of the IIR interpolation digital subfilters $H_a(z)$ and $H_b(z)$ constituent in the FRM IIR digital filter, a suitable analog reference filter $H_a(s)$ and its power complementary analog filter $H_b(s)$ have to be determined, where s is the analog frequency domain variable. Once $H_a(s)$ and $H_b(s)$ have been determined, the interpolation digital subfilters $H_a(z)$ and $H_b(z)$ are derived by using bilinear-LDI technique (see Section 6).

EMQF filters have several advantages for the design of FRM IIR digital filters. The squared ripple in the passband region of $H_a(z)$ and the squared ripple in the stopband region of $H_b(z)$ are equal as indicated by Eqn. (3). On the other hand, the squared ripple in the stopband region of $H_a(z)$ and the squared ripple in the passband region of $H_b(z)$ are equal. In addition, depending on whether the design specifications require a Case I or Case II FRM technique, either $H_a(z)$ or $H_b(z)$ could determine the maximum passband and stopband ripple of the overall FRM IIR digital filter $H(z)$. Consequently, the interpolation filter $H_a(z)$ is chosen to have equal passband and stopband squared tolerances. In this way, the resulting $H_b(z)$ also displays equal passband and stopband squared tolerances. These characteristics can be generalized for the analog reference subfilters $H_a(s)$ and $H_b(s)$. Therefore, there is a need for an analog reference filter $H_a(s)$ that together with its power complement $H_b(s)$ can exactly satisfy the passband and stopband relations in the FRM IIR filter. EMQF filters can successfully comply with the specifications present in the FRM IIR filter design. In addition, an EMQF transfer function can be easily designed by using bilinear-LDI transformation technique or any other structure consisting of two digital allpass networks in parallel. Furthermore, filters having EMQF transfer functions are minimally sensitive to component variations.

Despite all the advantages of EMQF filters, they suffer from not being able to independently specify passband and stopband ripples [41],[42] of the filter. Additionally, EMQF filters have exceedingly low passband attenuation.

All the poles of an EMQF transfer function reside on a circle in the s domain rendering them to have equal magnitudes. Given a squared passband and stopband tolerance of δ_p and δ_a, respectively, for an EMQF filter, the passband ripple Δ_p and minimum stopband attenuation Δ_a can be obtained as follows [43]:

$$\Delta_p = -10\log(1-\delta_p) \tag{16}$$

$$\Delta_a = -10\log(\delta_a) \tag{17}$$

The required passband and stopband edge frequencies for the analog reference filter $H_a(s)$ can be determined using design specifications along with Table 1. Frequency wrapping from digital to analog domain, and vice versa, has to be taken into account in accordance with:

$$\Omega_A = \frac{2}{T}\tan(\frac{\omega_d T}{2}) \tag{18}$$

where Ω_A is the analog frequency variable, where ω_d is the digital frequency variable, and where T is the sampling period.

Once the transfer function of the analog reference filter $H_a(s)$ is determined, it is represented as a sum of two allpass analog filters $G_0(s)$ and $G_1(s)$. In addition, $H_b(s)$, which is the power complementary of $H_a(s)$ is represented as the difference of $G_0(s)$ and $G_1(s)$. The poles of $G_0(s)$ and $G_1(s)$ are determined by cyclically distributing the poles of the reference filter $H_a(s)$ [43]. In the next section, belinear-LDI design technique is used to transform the two allpass networks $G_0(s)$ and $G_1(s)$ into digital domain.

6. Implementation of EMQF interpolation subfilters using bilinear-LDI design approach

In this section, the design procedure in [34, 44] is briefly explained to design and implement digital filters $G_0(z)$ and $G_1(z)$ using the the bilinear-LDI approach. This approach transforms analog reference filters $G_0(s)$ and $G_1(s)$ to obtain their digital filter counterparts $G_0(z)$ and $G_1(z)$.

The bilinear frequency transformation maps the analog frequency variable s to its digital domain counterpart z in accordance with:

$$s = \frac{2}{T}\frac{z-1}{z+1} \tag{19}$$

where T represents the sampling period, for mapping the transfer function of a prototype reference filter from the analog domain to the digital domain. The bilinear transform maps the left half of the complex s-plane to the interior of the unit circle in the z-plane. Therefore, BIBO stable filters in the s domain are converted to filters in the z domain which preserve that stability. Similarly, if the analog reference filter is minimum-phase, the previous characteristic of bilinear transform guarantees that the resulting digital filter is also minimum-phase. It also preserves the sensitivity properties of the analog

http://dx.doi.org/10.5772/52196

reference filter. However, bilinear transform may result in a digital filter that has delay-free loops in its implementation. Unfortunately, delay-free loops prevent the implementation of a digital filter to be realizable in hardware platform.

The LDI frequency transformation ensures the absence of delay-free loops in the digital implementation and is given by

$$s = \frac{1}{T}\left(z^{\frac{1}{2}} - z^{-\frac{1}{2}}\right) \tag{20}$$

The LDI frequency transformation maps the hardware implementation of the analog reference filter to digital domain. While the LDI frequency transformation guarantees that there are no delay-free loops in the implementation of the digital filter, it does this to the cost of resulting in a digital filter having poor magnitude-frequency responses. Moreover, it is incapable of preserving the BIBO stability properties of the analog reference filter.

The bilinear-LDI approach is a combination of the two above mentioned realization techniques. In bilinear-LDI transform, a precompensation is performed to the reference analog filter. Then, the conventional LDI design technique is applied to a network resulting from the precompensated analog prototype filter. The precompensation is such that the application of the LDI design technique results in a filter that exactly matches the bilinear frequency transform of the uncompensated analog prototype filter.

The resulting bilinear-LDI digital filters have several desirable features from a hardware realization point of view. They are minimal in the number of digital multiplication operations. Although they are not minimal in the number of digital adders and unit-delays, the additional adders and the additional unit delay lead to certain advantages when the concept of generalized delay unit is used for the realization of the network [34]. Moreover, The bilinear-LDI digital filters lend themselves to fast two-cycle parallel digital signal processing speeds and they exhibit exceptionally low passband sensitivity to their multiplier coefficient values, resulting in small coefficient wordlengths.

As discussed in Section 5, the analog reference filter $H_a(s)$ is decomposed into two allpass analog networks $G_0(s)$ and $G_1(s)$. The digital allpass networks $G_0(z)$ and $G_1(z)$ are obtained from $G_0(s)$ and $G_1(s)$ using the bilinear-LDI design approach.

It should be pointed out that $G_0(s)$ is an odd-ordered allpass function. Therefore, it has a pole on the real axis in the s domain. On the other hand, $G_1(s)$ ends up having an even-ordered allpass function. It is well known that an allpass transfer function can be written in the general form [34]:

$$G(s) = \frac{P(-s)}{P(s)} \tag{21}$$

where $P(s)$ is a Hurwitz polynomial of order, say, $\tilde{n}$. Moreover, $P(s)$ can be expressed as:

$$P(s) = \mathrm{Ev}P(s) + \mathrm{Od}P(s) \tag{22}$$

where $\mathrm{Ev}P(s)$ denotes the even and $\mathrm{Od}P(s)$ denotes the odd part of $P(s)$.

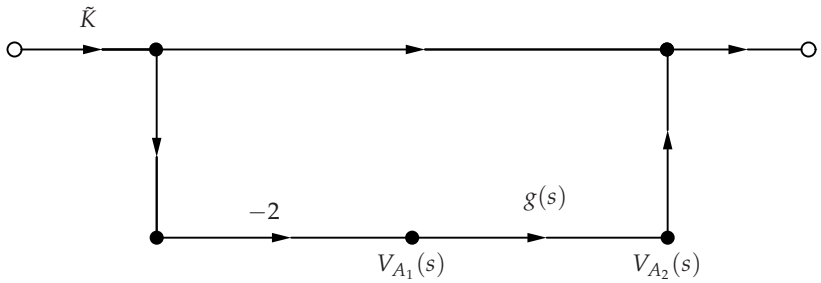

Figure 9. Signal Flow Graph of $G(s)$

By simple manipulation of Eqns. (21) and (22) one can get

$$G(s) = \tilde{K}\frac{1 - Z(s)}{1 + Z(s)} \tag{23}$$

Here, $\tilde{K} = 1$ or -1, and $Z(s)$ is a realizable reactive impedance given by

$$Z(s) = \begin{cases} \dfrac{\mathrm{Od}P(s)}{\mathrm{Ev}P(s)} & \text{for even } \tilde{n} \\ \dfrac{\mathrm{Ev}P(s)}{\mathrm{Od}P(s)} & \text{for odd } \tilde{n} \end{cases} \tag{24}$$

where $\tilde{n}$ is the order of $G(s)$ (odd when realizing $G_0(s)$ and even when realizing $G_1(s)$). The impedance $Z(s)$ has a zero at $s = 0$ for even $\tilde{n}$ and a pole at $s = 0$ for odd $\tilde{n}$, while having a zero at $s = \infty$ both for even $\tilde{n}$ and for odd $\tilde{n}$.

The bilinear-LDI digital realization of $G(s)$ is achieved by using the following steps:

- The transfer function $G(s)$ is decomposed in the form

$$G(s) = \tilde{K}[1 - 2g(s)] \tag{25}$$

where

$$g(s) = \frac{Z(s)}{1 + Z(s)} \tag{26}$$

Here, $G(s)$ can be realized as the transfer function of the signal-flow graph in Fig. 9.

Furthermore, $g(s)$ represents a lowpass or highpass analog filter that can be realized as the transfer function of the voltage divider network in Fig. 10.

http://dx.doi.org/10.5772/52196

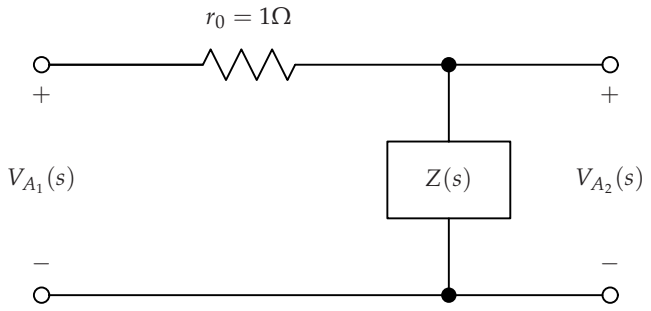

Figure 10. Voltage Divider Circuit for $g(s)$

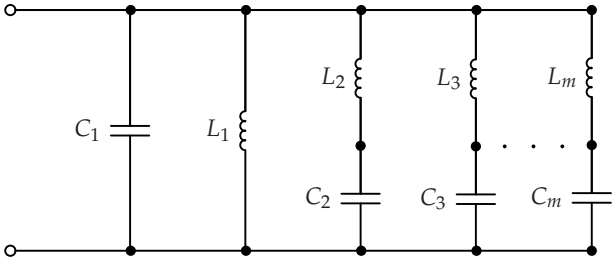

Figure 11. Realization of Impedance $Z(s)$

Finally, $Z(s)$ represents realizable reactances (consisting of capacitors and inductors only) and can be decomposed into its Foster II canonical form, as in Fig. 11, in accordance with

$$Z(s) = \frac{1}{Y(s)} \tag{27}$$

$$Y(s) = sC_1 + \frac{1}{sL_1} + \sum_{i=2}^{m} \frac{sC_i}{s^2 C_i L_i + 1} \tag{28}$$

where $m = \tilde{n}/2$ for even $\tilde{n}$ and $m = (\tilde{n}+1)/2$ for odd $\tilde{n}$, and where C_i represent capacitances and L_i represent inductances (for $i = 1, 2, \ldots, m$), and inductor L_1 is only present for even $\tilde{n}$.

- The impedance $Z(s)$ in Fig. 11 is substituted into Fig. 10 and the precompensation is applied to the resulting network. This amounts to a modification of circuit elements in accordance with:

$$V'_{A_1}(s) = \frac{V_{A_1}(s)}{1 - sT/2} \tag{29}$$

The resistance in r_0 in Fig. 10 is modified to:

$$r'_0 = z^{\frac{1}{2}} r_0 \tag{30}$$

and

$$L_1^{'} = L_1 \tag{31}$$

$$C_1^{'} = C_1 + \frac{T}{2} + \frac{T^2}{4L_1} + \sum_{i=2}^{m} \frac{C_i \frac{T^2}{4L_i}}{C_i + \frac{T^2}{4L_i}} \tag{32}$$

$$L_i^{'} = L_i \left[\frac{C_i + \frac{T^2}{4L_i}}{C_i} \right]^2 \tag{33}$$

$$C_i^{'} = \frac{C_i^2}{C_i + \frac{T^2}{4L_i}} \tag{34}$$

with $r_0 = 1\Omega$ and for $i = 2, 3, ..., m$.

- Since the voltage/current signal-flow graph of the precompensated network [34] consists of analog integrators only and it has no analog differentiators, it can be used for bilinear-LDI realization method. Therefore, the analog integrators in the signal-flow graph of the precompensated network are replaced by LDI digital integrators, and by impedance-scaling, the resulting network is scaled by $z^{-\frac{1}{2}}$ to eliminate any half-delay elements. The resulting digital network is displayed in Fig. 12. The multiplier coefficients in Fig. 12 are as follows:

$$m_{L_i} = \frac{T}{L_i^{'}} \tag{35}$$

$$m_{C_i} = \frac{T}{C_i^{'}} \tag{36}$$

for $i = 1, 2, ..., m$.

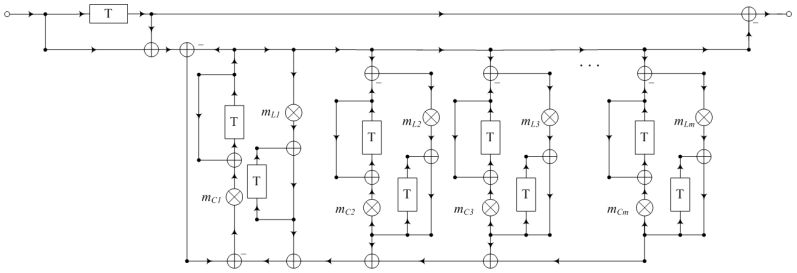

Figure 12. Realization of the Bilinear-LDI Digital Allpass Network $G(z)$ [34]

http://dx.doi.org/10.5772/52196

7. Constraints for guaranteed BIBO stability

In order for the FRM digital filter consisting of CSD multiplier coefficients $\hat{m}_{FRM}$ to be BIBO stable, it is both necessary and sufficient for the bilinear-LDI IIR interpolation digital subfilters $H_a(z)$ and $H_b(z)$ to be BIBO stable. Likewise, in order for the interpolation digital subfilters $H_a(z)$ and $H_b(z)$ to be BIBO stable, it is both necessary and sufficient for the bilinear-LDI allpass digital networks $G_0(z)$ and $G_1(z)$ to be BIBO stable. In this way, it is required that the bilinear-LDI digital allpass networks $G_0(z)$ and $G_1(z)$ remain BIBO stable throughout the course of the PSO algorithm.

In the course of PSO algorithm, the infinite-precision multiplier coefficients m_{L_i} and m_{C_i} can only take quantized values $\hat{m}_{L_i}$ and $\hat{m}_{C_i}$ that belong to $CSD(L,l,f)$. In order for the bilinear-LDI digital allpass networks $G_0(z)$ and $G_1(z)$ to remain BIBO stable, it is required that the values of the corresponding quantized reactive elements $\hat{L}_i$ and $\hat{C}_i$ remain positive [45] in the course of optimization. This is due to the properties of the bilinear frequency transformation from analog to digital domain. In order to find the conditions for BIBO stability and in accordance with Eqns. (35) and (36), one has:

$$\hat{L}_i^{'} = \frac{T}{\hat{m}_{L_i}} \tag{37}$$

$$\hat{C}_i^{'} = \frac{T}{\hat{m}_{C_i}} \tag{38}$$

Moreover, in accordance with Eqns. (31-34), one has:

$$\hat{L}_1^{'} = \hat{L}_1 \tag{39}$$

$$\hat{C}_1^{'} = \hat{C}_1 + \frac{T}{2} + \frac{T^2}{4\hat{L}_1} + \sum_{i=2}^{m} \frac{\hat{C}_i \frac{T^2}{4\hat{L}_i}}{\hat{C}_i + \frac{T^2}{4\hat{L}_i}} \tag{40}$$

$$\hat{L}_i^{'} = \hat{L}_i \left[\frac{\hat{C}_i + \frac{T^2}{4\hat{L}_i}}{\hat{C}_i} \right]^2 \tag{41}$$

$$\hat{C}_i^{'} = \frac{\hat{C}_i^2}{\hat{C}_i + \frac{T^2}{4\hat{L}_i}} \tag{42}$$

where $\hat{L}_1 = \infty$ for odd-ordered allpass network $G_0(z)$.

By substituting Eqns. (37) and (38) into Eqns. (39-42), and by solving the resulting equations for the reactive elements $\hat{L}_i$ and $\hat{C}_i$, one can obtain

$$\hat{L}_1 = \frac{T}{\hat{m}_{L_1}} \tag{43}$$

$$\hat{C}_1 = \frac{T\left\{\frac{4}{\hat{m}_{C_1}} - \hat{m}_{L_1} - 4\left(\sum_{i=2}^{m} \frac{1}{\frac{4}{\hat{m}_{L_i}} - \hat{m}_{C_i}}\right) - 2\right\}}{4} \tag{44}$$

$$\hat{L}_i = \frac{T(\hat{m}_{L_i}\hat{m}_{C_i} - 4)^2}{16\hat{m}_{L_i}} \tag{45}$$

$$\hat{C}_i = \frac{-4T}{\hat{m}_{C_i}(\hat{m}_{L_i}\hat{m}_{C_i} - 4)} \tag{46}$$

From Eqns. (43-46), $\hat{L}_i > 0$ and $\hat{C}_i > 0$ provide that

$$\hat{m}_{L_1} > 0 \tag{47}$$

$$\hat{m}_{L_i} > 0 \tag{48}$$

$$\hat{m}_{C_i} < \frac{4}{\hat{m}_{L_i}} \tag{49}$$

$$\hat{m}_{C_1} < \frac{4}{\left\{\hat{m}_{L_1} + 4\left(\sum_{i=2}^{m} \frac{1}{\frac{4}{\hat{m}_{L_i}} - \hat{m}_{C_i}}\right) + 2\right\}} \tag{50}$$

Then, in order to make the CSD FRM digital filter BIBO stable, it is necessary and sufficient to choose the values of the multiplier coefficients $\hat{m}_{FRM} \in CSD(L,l,f)$ such that the inequality constraints (47-50) are satisfied. The equations and corresponding condition required for BIBO stability are summarized in Table 2.

In order to make the CSD lowpass digital IIR FRM filter BIBO stable, it is necessary and sufficient to choose the values of the multiplier coefficients $\hat{m}_{L_i}$, $\hat{m}_{C_i} \in CSD(L,l,f)$ such that the inequality constraints of Table 2 are satisfied.

It should be pointed out that constraint (49) is most stringent when $\hat{m}_{L_i}$ is at its largest possible value. Similarly, constraint (50) is most stringent when $\hat{m}_{L_1}$, $\hat{m}_{L_i}$ and $\hat{m}_{C_i}$ are all at their largest possible values (while $\hat{m}_{L_i}$ and $\hat{m}_{C_i}$ still adhere to constraint $\hat{m}_{C_i} < 4\,(\hat{m}_{L_i})^{-1}$).

8. Proposed PSO of FRM IIR digital filters

The proposed particle swarm optimization of BIBO stable FRM IIR digital filters is carried out over the CSD multiplier coefficient space $CSD(L_{0\,\text{or}\,1}, l_{0\,\text{or}\,1}, f_{0\,\text{or}\,1})$, where $L_{0\,\text{or}\,1}$ represents the multiplier coefficient wordlength, where $l_{0\,\text{or}\,1}$ represents the maximum number of non-zero digits, and where $f_{0\,\text{or}\,1}$ represents the number of fractional part digits (for FIR or IIR digital subfilters, respectively).

http://dx.doi.org/10.5772/52196

Element	Equation	Inequality Constraints
$\hat{L}_1$	$\frac{T}{\hat{m}_{L_1}}$	$\hat{m}_{L_1} > 0$
$\hat{C}_1$	$\frac{1}{4}T\left\{\frac{4}{\hat{m}_{C_1}} - \hat{m}_{L_1} - 4\left(\sum_{i=2}^{m}\frac{1}{\frac{4}{\hat{m}_{L_i}} - \hat{m}_{C_i}}\right) - 2\right\}$	$\hat{m}_{C_1} < 4\left\{\hat{m}_{L_1} + 4\left(\sum_{i=2}^{m}\frac{1}{\frac{4}{\hat{m}_{L_i}} - \hat{m}_{C_i}}\right) + 2\right\}^{-1}$
$\hat{L}_i$	$\frac{T(\hat{m}_{L_i}\hat{m}_{C_i} - 4)^2}{16\hat{m}_{L_i}}$	$\hat{m}_{L_i} > 0$
$\hat{C}_i$	$\frac{-4T}{\hat{m}_{C_i}(\hat{m}_{L_i}\hat{m}_{C_i} - 4)}$	$\hat{m}_{C_i} < 4\,(\hat{m}_{L_i})^{-1}$

Table 2. Relations for Elements of Back-Transformed Reactance

The starting point of any stochastic algorithm plays an important role in the convergence behavior of the optimization algorithm [46]. Therefore, it is important to generate the initial swarm in proper positions in the search space rather than complete random generation of the initial population. In order to achieve this, the following technique is employed:

8.1. Initiation of PSO

To start the PSO algorithm from a good position in the search space the infinite precision multiplier coefficient values of the seed particle are generated by using classical techniques as discussed in previous sections. These infinite precision multiplier coefficient values are turned into their finite precision counterparts by simply rounding them to their closest CSD values. This seed particle is used as the center of the swarm and a cloud of particles are generated randomly around the seed particle. It should be noted that the distance of the randomly generated particles should not be far from the seed particle. In this way, the initial swarm contains particles which have high chances of being near the optimal solution. The multiplier coefficient values of the swarm are taken from a set of CSD LUTs which are constructed as follows:

8.2. FRM IIR digital filter template LUTs

It is necessary and sufficient to choose the values of the multiplier coefficients, such that the inequality constraints (47-50) are satisfied. In order to achieve this, the LUTs are constructed as follows:

- One LUT is constructed for all multiplier coefficient values $\hat{m}_{FIR} \in CSD(L_0, l_0, f_0)$ for the masking digital subfilters $F_0(z)$ and $F_1(z)$. The values of L_0, l_0 and f_0 are determined empirically based on the amplitude frequency-response of the masking digital subfilters $F_0(z)$ and $F_1(z)$.
- A LUT is constructed for all multiplier coefficient values $\hat{m}_{IIR} \in CSD(L_1, l_1, f_1)$ for the digital allpass networks $G_0(z)$ and $G_1(z)$. Once again, the values of L_1, l_1 and f_1 are determined empirically. Also, it is expedient to assume that $\hat{m}_{IIR}$ have only positive values.
- The above CSD LUT is used to form one size-reduced LUT per the multiplier coefficient for digital allpass networks $G_0(z)$ and $G_1(z)$, where each size-reduced LUT initially includes CSD values bounded from below by the smallest representable value belonging to $CSD(L_1, l_1, f_1)$, and

from above by the corresponding value of the finite-wordlength coefficients for the seed particle. The size-reduced LUTs are augmented before PSO process commences. The purpose of this augmentation is to ensure that the exploration space include as many of those CSD multiplier coefficients $\hat{m}_{L_1}$, $\hat{m}_{C_1}$, $\hat{m}_{L_i}$ and $\hat{m}_{C_i}$ which still satisfy the BIBO stability constraints (47-50).

The above constructed LUTs are used as template LUTs. There are two problems concerning the PSO of FRM IIR digital filters over the CSD multiplier coefficient space. To overcome these problems, the template LUTs must be further processed. These two problems and the way to solve them are discussed in the following.

8.3. PSO indirect search method

In PSO, the required new particle position is obtained from the previous position of the particle through the addition of a random (normalized) velocity value. However, by directly applying the conventional PSO to the above optimization over the CSD multiplier coefficients, one may obtain new particle positions whose coordinate values are no longer in $CSD(L_{0\,\text{or}\,1}, l_{0\,\text{or}\,1}, f_{0\,\text{or}\,1})$. In order to overcome this problem, the optimization search is carried out indirectly via the indices to the LUT CSD values (as opposed to LUT CSD values themselves). In this way, the CSD coordinate values for each particle position are obtained by integer indices to the CSD LUTs. The key point in the indirect search rests with ensuring that the index set is closed, i.e. by ensuring that each index points to a valid CSD value in the LUT, and that the resulting particle in the course of PSO adheres to the prespecified CSD number format.

If the velocity values are replaced by their closest integer values, the update equations become modified to

$$\hat{v}_{kj}^{i} = [w\hat{v}_{kj}^{i-1} + c_1 r_1(\hat{x}_{best_{kj}}^{i-1} - \hat{x}_{kj}^{i-1}) + c_2 r_2(\hat{g}_{best_j}^{i-1} - \hat{x}_{kj}^{i-1})]^{1} \tag{51}$$

$$\text{if} \quad \hat{v}_{kj}^{i} < \hat{v}_{min} \quad ; \quad \hat{v}_{kj}^{i} = \hat{v}_{min}$$

$$\text{if} \quad \hat{v}_{kj}^{i} > \hat{v}_{max} \quad ; \quad \hat{v}_{kj}^{i} = \hat{v}_{max}$$

$$\hat{x}_{kj}^{i} = \hat{x}_{kj}^{i-1} + \hat{v}_{kj}^{i} \tag{52}$$

Here, $\hat{x}_{kj}$, $\hat{v}_{kj}$, $\hat{x}_{best_{kj}}$, $\hat{g}_{best_j}$, $\hat{v}_{min}$ and $\hat{v}_{max}$ are all integer values where $\hat{v}_{min} < 0$ and $\hat{v}_{max} > 0$. In addition, w is limited in the interval $[0, 0.5)$ (as discussed shortly).

8.4. Barren layers

Due to their finite length, the template LUTs inevitably lead to a bounded optimization search space. In order to ensure that the particles do not cross over to the outside of the search space in the course of PSO, the search space is constructed as a combination of two regions, namely the interior and barren layers. The barren layer is constructed to yield relatively low fitness values, and is represented as header and footer in the template LUT. There are two problems concerning the construction of the barren layers:

[1] $[R]$ denotes rounding R to its closest integer, where R is assumed to be a real value.

http://dx.doi.org/10.5772/52196

8.4.1. barren layer entries

The first problem in the construction of barren layers concerns how to make the fitness values in the barren layer relatively low. This problem can be resolved by filling the header part by unrealistically large, and the footer part by unrealistically small CSD multiplier coefficient values.

8.4.2. barren layer width

The second problem, on the other hand, concerns how to determine the width of the barren layer such that the particles do not cross over to the outside of the search space even under the worst case scenario. These two problems relate to the number of entries and the CSD values of the entries in header and footer parts of the template LUTs. To overcome this problem, let us consider the j-th variable in the k-th particle is in the boundaries of one of the template LUTs in iteration $i-1$. The worst case scenario occurs when x_{kj}^{i-1} moves toward the barren layer with the peak permissible velocities (v_{max} for the header, and v_{min} for the footer). If in the i-th iteration x_{kj}^{i} is in the footer:

$$\hat{x}_{best_{kj}}^{i} > \hat{x}_{kj}^{i} \tag{53}$$

$$\hat{g}_{best_{j}}^{i} > \hat{x}_{kj}^{i} \tag{54}$$

and if it is in the header:

$$\hat{x}_{best_{kj}}^{i} < \hat{x}_{kj}^{i} \tag{55}$$

$$\hat{g}_{best_{j}}^{i} < \hat{x}_{kj}^{i} \tag{56}$$

Eqns. (53-56) show that the velocity of the particle in iteration $i+1$ tends to move the particle in a direction opposite to the direction of the barren regions. Here, the worst case happens when $r_1 = r_2 = 0$. In this way, the number of entries L_f in the footer part, and the number of entries L_h in the header part is determined in accordance with

$$\begin{aligned} L_f &= |\hat{v}_{min}| + [w|\hat{v}_{min}|] + [w[w|\hat{v}_{min}|]] + \dots \\ &\leq |\hat{v}_{min}| + \frac{|\hat{v}_{min}|}{2} + \frac{|\hat{v}_{min}|}{4} + \dots \\ &= 2|\hat{v}_{min}| \end{aligned} \tag{57}$$

$$\begin{aligned} L_h &= \hat{v}_{max} + [w\hat{v}_{max}] + [w[w\hat{v}_{max}]] + \dots \\ &\leq \hat{v}_{max} + \frac{\hat{v}_{max}}{2} + \frac{\hat{v}_{max}}{4} + \dots \\ &= 2\hat{v}_{max} \end{aligned} \tag{58}$$

Let us recall that since $0 \leq w < 0.5$,

$$\text{if} \quad v : \text{positive integer} \quad \Rightarrow \quad [wv] \leq \frac{v}{2} \tag{59}$$

In addition, after some iterations $\hat{v}_{kj}^{i+1} = 0$. Otherwise, if $w \geq 0.5$, $\hat{v}_{kj}^{i+1}$ can never become zero, and the width of the barren layer will be infinity.

The augmented LUTs remains fixed in the course of PSO, restricting automatic particle movement inside the limited search space. Modifying the index values inside each particle by adding the current indices to the length of the footer barren region, L_f, PSO algorithm is ready to start the optimization of FRM digital filters.

9. Design methodology

The design methodology for the proposed PSO of BIBO stable bilinear-LDI based FRM IIR digital filters over the CSD multiplier coefficient space can be summarized as follows:

1. *Designing the interpolation digital subfilter*: the first step in determining the interpolation subfilter specifications is to fix the interpolation factor M from a pre-specified range. This is done in a way that the order of the FIR masking filters is kept minimal. Using the passband edge frequency ω_p and stopband edge frequency ω_a and the expressions for boundary frequencies given in Table 1, one can determine the filter case and calculate the approximate passband edge $\tilde{\theta}$ and stopband edge $\tilde{\phi}$ of the digital interpolation lowpass subfilter $H(e^{j\omega})$, for every value of the user specified range of interpolation factors M. The order of the FIR masking filters depends on the minimum distance between consecutive image replicas of either the interpolated subfilter $H_a(e^{jM\omega})$ or its complement $H_b(e^{jM\omega})$. Then, displacement λ_M and distance $\tilde{D}_M$ for each interpolation factor M are given as:

$$\lambda_M = \max[|(\frac{\pi}{2} - \tilde{\theta})|, |(\frac{\pi}{2} - \tilde{\phi})|] \tag{60}$$

$$\tilde{D}_M = \frac{\pi}{M} - \frac{2\lambda}{M} \tag{61}$$

To minimize the length of FIR-masking filters, the value of M that results in the largest value of $\tilde{D}_M$ is chosen. This determines the optimal interpolation factor M as well as the approximate passband edge $\tilde{\theta}$ and stopband edge $\tilde{\phi}$ of the digital interpolation subfilter $H(e^{j\omega})$. EMQF filters have the property of equal square magnitude ripple size in the passband and stopband. Therefore, of the two ripple specifications, whichever gives the smallest tolerance in the squared magnitude response determines both the passband ripple R_p and stopband attenuation R_a of the interpolation digital subfilter $H_a(e^{j\omega})$. The interpolation digital subfilter order N_{IIR} is then determined using R_p, R_a, $\tilde{\theta}$ and $\tilde{\phi}$. N_{IIR} must be rounded to the nearest larger odd integer so that it can be implemented by a parallel combination of two allpass networks. With the order N_{IIR}, and passband and stopband ripples R_p and R_a fixed, the ratio of the analog passband edge θ_A and stopband edge ϕ_A is a constant k given by [47]

$$D = \frac{10^{0.1R_a} - 1}{10^{0.1R_p} - 1}$$

$$q = 10^{\frac{-\log(16D)}{N_{IIR}}}$$

http://dx.doi.org/10.5772/52196

$$q = q_0 + 2q_0^5 + 15q_0^9 + 150q_0^{13}$$

$$k_p = \left[\frac{1-2q_0}{1+2q_0}\right]^2$$

$$k = \sqrt{1-k_p^2}$$

In order to satisfy the passband edge specification, the digital passband edge $\omega_p = \tilde{\theta}$ for Case I filters. The digital stopband edge ω_a is then determined using the analog ratio k. (Here, frequency warping from digital to analog domain, and vice versa, given by Eqn. (18) needs to be taken into account.) Similarly, $\omega_a = \tilde{\phi}$ for Case II filters, and ω_p can be determined by using ratio k. Also, using given ripple specifications along with the boundary frequencies described in Table 1, one can determine the transfer function of the FIR masking filters $F_0(e^{j\omega})$ and $F_1(e^{j\omega})$.

2. *Generation of seed FRM digital filter particle*: The seed FRM digital filter particle is formed as follows:
   - A particle with B_1 coordinates is formed in which each coordinate serves as an index of the corresponding CSD LUT for each multiplier coefficient constituent in the interpolation digital subfilters. For FRM IIR digital filters, the multiplier coefficients correspond to the bilinear-LDI allpass digital networks $G_0(z)$ and $G_1(z)$.
   - A particle with B_2 coordinates is formed in which each coordinate serves as an index of the corresponding CSD LUT for each multiplier coefficient in the FIR masking digital subfilters $F_0(z)$ and $F_1(z)$.
3. *Generation of Initial Swarm*: An initial swarm of K particles is formed by generating a random cloud around the seed particle as discussed in section 8.1.
4. *Fitness Evaluation*: The fitness function for CSD FRM IIR digital filters is defined in accordance with

$$fitness_{magnitude} = -20log[max(\varepsilon_p, \varepsilon_a)] \tag{62}$$

$$fitness_{group-delay} = \varsigma_p \tag{63}$$

$$fitness = fintess_{magnitude} - fitness_{group-delay} \tag{64}$$

where

$$\varepsilon_p = \underbrace{max}_{\omega \in \Delta\omega_p} [W_p |H(e^{j\omega}) - 1|] \tag{65}$$

$$\varepsilon_a = \underbrace{max}_{\omega \in \Delta\omega_a} [W_a |H(e^{j\omega})|] \tag{66}$$

$$\varsigma_p = \underbrace{max}_{\omega \in \Delta\omega_p} [W_{gd} |\tau(\omega) - \mu_\tau|] \tag{67}$$

with $\Delta\omega_p$ representing the passband frequency region(s), with $\Delta\omega_a$ representing the stopband frequency region(s), and with $\tau(\omega)$ representing the group-delay frequency response of the FRM IIR digital filter. Here, W_p, W_a, and W_{gd} represent weighting factors for the passband and stopband magnitude responses, and for the group-delay response, respectively. Moreover, μ_τ represents the average group-delay over the passband region.

In [48], a convenient way to represent digital networks in terms of matrix representation is presented. This technique can be used to find the magnitude and group delay frequency response of the digital network in Fig. 12. Let us consider the input to the digital network in Fig. 12 to be x_D and the output of it to be y_D. In addition, let the output of the i-th time delay in Fig. 12 to be x_i and the input to the i-th time delay to be y_i. The transfer function matrix of the network, $\mathbf{T}$, can be found as

$$\mathbf{y} = \mathbf{T}\mathbf{x} \tag{68}$$

where $\mathbf{y} = [y_D, y_1, y_2, \ldots, y_{2m+1}]^t$ [2] and $\mathbf{x} = [x_D, x_1, x_2, \ldots, x_{2m+1}]^t$, and $\mathbf{T}$ is a $(2m+2) \times (2m+2)$ matrix with the entries obtained as Eqn. (69).

$$\mathbf{T} = \begin{bmatrix}
0 & 1 & -1 & 0 & 0 & 0 & \ldots & 0 & 0 \\
1 & 0 & 0 & 0 & 0 & 0 & \ldots & 0 & 0 \\
m_{C_1} & m_{C_1} & 1-m_{C_1}(1+\sum_{i=1}^{m} m_{L_i}) & -m_{C_1} & m_{C_1}m_{L_2} & -m_{C_1} & \ldots & m_{C_1}m_{L_m} & -m_{C_1} \\
0 & 0 & m_{L_1} & 1 & 0 & 0 & \ldots & 0 & 0 \\
0 & 0 & m_{C_2}m_{L_2} & 0 & 1-m_{C_2}m_{L_2} & m_{C_2} & \ldots & 0 & 0 \\
0 & 0 & m_{L_2} & 0 & -m_{L_2} & 1 & \ldots & 0 & 0 \\
\vdots & \vdots & \vdots & \vdots & \vdots & \vdots & \ddots & & \\
0 & 0 & m_{C_m}m_{L_m} & 0 & 0 & 0 & & 1-m_{C_m}m_{L_m} & m_{C_m} \\
0 & 0 & m_{L_m} & 0 & 0 & 0 & & -m_{L_m} & 1
\end{bmatrix} \tag{69}$$

Since $x_i = z^{-1}y_i$, the transfer function $G(z) = \frac{y_D}{x_D}$ can be found as

$$G(z) = z^{-1}\mathbf{e}[\mathbf{I} - z^{-1}\mathbf{D}]^{-1}\mathbf{c} \tag{70}$$

where $\mathbf{e}$ is a row vector and $\mathbf{c}$ is a column vector of length $2m+1$, and where $\mathbf{I}$ is the identity matrix and $\mathbf{D}$ is a $(2m+1) \times (2m+1)$ matrix in accordance with

$$\mathbf{T} = \begin{bmatrix} 0 & \mathbf{e} \\ \mathbf{c} & \mathbf{D} \end{bmatrix} \tag{71}$$

[2] $\mathbf{X}^t$ denotes the transpose of the matrix $\mathbf{X}$.

http://dx.doi.org/10.5772/52196

The matrix $\mathbf{T}$ is also useful in finding the group delay of $H(z)$. The group-delay of $H(e^{j\omega})$ is given by

$$\tau(\omega) = -\mathrm{Im}\left\{\frac{1}{H(e^{j\omega})}\frac{dH(e^{j\omega})}{d\omega}\right\} \tag{72}$$

With the help of Eqn. (12), the expression $\frac{dH(e^{j\omega})}{d\omega}$ can be written as

$$\begin{aligned}\frac{dH(e^{j\omega})}{d\omega} = \frac{1}{2}\Big[&\frac{dG_0(e^{j\omega})}{d\omega}(F_0(e^{j\omega}) + F_1(e^{j\omega})) + \\ &\frac{d(F_0(e^{j\omega}) + F_1(e^{j\omega}))}{d\omega}G_0(e^{j\omega}) + \\ &\frac{dG_1(e^{j\omega})}{d\omega}(F_0(e^{j\omega}) - F_1(e^{j\omega})) + \\ &\frac{d(F_0(e^{j\omega}) - F_1(e^{j\omega}))}{d\omega}G_1(e^{j\omega})\Big]\end{aligned} \tag{73}$$

The derivative of FIR filters can be easily found from their transfer function. In order to find the derivative of the digital allpass networks $G_0(z)$ and $G_1(z)$, the following expression can be used

$$\frac{dG(e^{j\omega})}{d\omega} = -je^{-j\omega}\sum_{i=1}^{2m+1} G_{xi}(e^{j\omega})G_{iy}(e^{j\omega}) \tag{74}$$

where $G_{xi}(z)$ is the transfer function between x_D and y_i, and where $G_{iy}(z)$ is the transfer function between x_i and y_D. The transfer functions $G_{xi}(z)$ and $G_{iy}(z)$ can be found from the transfer function matrix $\mathbf{T}$ as follows

$$G_{xi}(z) = a_{xi} + z^{-1}\mathbf{e}_{xi}[\mathbf{I} - z^{-1}\mathbf{D}]^{-1}\mathbf{c} \tag{75}$$

$$G_{iy}(z) = a_{iy} + z^{-1}\mathbf{e}[\mathbf{I} - z^{-1}\mathbf{D}]^{-1}\mathbf{c}_{iy} \tag{76}$$

where a_{xi} and a_{iy} are scalars, $\mathbf{e}_{xi}$ is a row vector and $\mathbf{c}_{iy}$ is a column vector of length $2m+1$, in accordance with $[a_{xi} \quad \mathbf{e}_{xi}]$ is the i-th row of the matrix $\mathbf{T}$, and $[a_{iy} \quad \mathbf{c}_{iy}^t]^t$ is the i-th column of the matrix $\mathbf{T}$. Having the expressions for $H(e^{j\omega})$ and $\frac{dH(e^{j\omega})}{d\omega}$, the group delay can be obtained in accordance with Eqn. (72).

The passband and stopband weighting factors W_p and W_a are easily determined from user specifications. The group-delay weighting factor is set as

$$W_{gd} = \frac{\zeta \times fitness_{magnitude}}{fitness_{group-delay}} \tag{77}$$

where ζ is a fixed constant such that $0 < \zeta < 1$, and where $fitness_{magnitude}$ and $fitness_{group-delay}$ are obtained by examining the seed FRM digital filter particle. The weighting factor for the group-delay increases as $\zeta \to 1$.

Maximum Passband Ripple A_p	0.1[dB]
Minimum Stopband Loss A_a	40[dB]
Lower Stopband-Edge Normalized Frequency ω_{a_1}	0.31π[Rad]
Lower Passband-Edge Normalized Frequency ω_{p_1}	0.33π[Rad]
Upper Passband-Edge Normalized Frequency ω_{p_2}	0.60π[Rad]
Upper Stopband-Edge Normalized Frequency ω_{a_2}	0.61π[Rad]
Normalized Sampling Period T	1[s]
Lowpass Filter Interpolation Factor M_{lp}	6
Highpass Filter Interpolation Factor M_{hp}	5

Table 3. Design Specifications for Bandpass FRM IIR Digital Filter

K	w	c_1	c_2	$\hat{v}_{min}$	$\hat{v}_{max}$	L_f	L_h
700	0.4	2	2	-5	5	10	10

Table 4. PSO Design Parameters for Bandpass FRM IIR Digital Filter

L_0	l_0	f_0	L_1	l_1	f_1
11	3	10	12	3	7

Table 5. CSD Parameters for Bandpass FRM IIR Digital Filter

10. Application examples

10.1. Bandpass FRM IIR digital filter design example

Consider the design of a bandpass FRM IIR digital filter satisfying the magnitude response design specifications given in Table 3 over the CSD multiplier coefficient space.

The parameters for the PSO of bandpass FRM IIR digital filter is shown in Table 4 and the CSD parameters are presented in Table 5.

Given the design specification in Table 3, The order of the digital allpass networks $G_{0_{lp}}(z)$, $G_{1_{lp}}(z)$, $G_{0_{hp}}(z)$ and $G_{1_{hp}}(z)$ are found to be 3, 4, 3 and 4, respectively. In addition, the digital masking subfilters $F_{0_{lp}}(z)$, $F_{1_{lp}}(z)$, $F_{0_{hp}}(z)$ and $F_{1_{hp}}(z)$ have the same length as the previous example, i.e. 24, 42, 25 and 35 respectively, resulting in $N = 140$. In this example a set of fifteen CSD LUTs are required, fourteen LUTs for the multiplier coefficients $m_{C_{0,1}}$, $m_{C_{0,2}}$, $m_{C_{0,3}}$, $m_{L_{0,2}}$, $m_{L_{0,3}}$, $m_{C_{1,1}}$, $m_{L_{1,1}}$, $m_{C_{1,2}}$ and $m_{L_{1,2}}$ constituent in the digital allpass networks $G_{0_{lp}}(z)$, $G_{1_{lp}}(z)$, $G_{0_{hp}}(z)$ and $G_{1_{hp}}(z)$, and one template LUT for all the multiplier coefficients constituent in the masking digital subfilters $F_{0_{lp}}(z)$, $F_{1_{lp}}(z)$, $F_{0_{hp}}(z)$ and $F_{1_{hp}}(z)$.

Finally, by using Parks McClellan approach, the subfilters $F_{0_{lp}}(z)$, $F_{1_{lp}}(z)$, $F_{0_{hp}}(z)$ and $F_{1_{hp}}(z)$ can be designed. Also, by using the EMQF technique, the digital allpass networks $G_{0_{lp}}(z)$, $G_{1_{lp}}(z)$, $G_{0_{hp}}(z)$ and $G_{1_{hp}}(z)$ can be designed. Consequently, the magnitude and group delay frequency responses of the overall infinite-precision bandpass FRM IIR digital filter $H(z)$ is obtained as shown in Figs. 13 and 14.

http://dx.doi.org/10.5772/52196

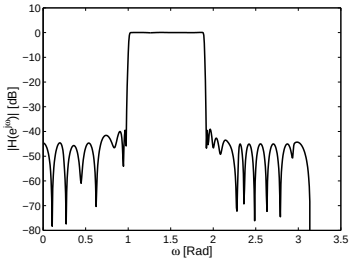

Figure 13. Magnitude Frequency-Response of the Overall Infinite-Precision Bandpass FRM IIR Digital Filter $H(e^{j\omega})$

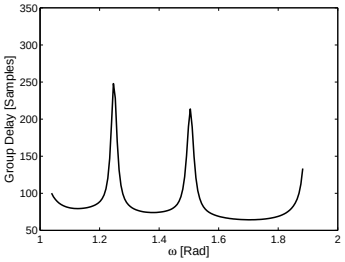

Figure 14. Group Delay Frequency-Response of the Overall Infinite-Precision Bandpass FRM IIR Digital Filter $H(e^{j\omega})$

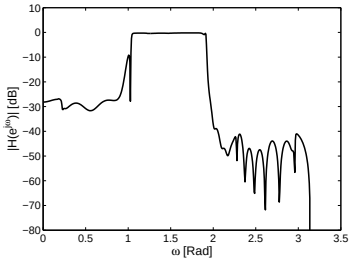

Figure 15. Magnitude Frequency-Response of the Overall CSD Bandpass FRM IIR Digital Filter $H(e^{j\omega})$ Before PSO

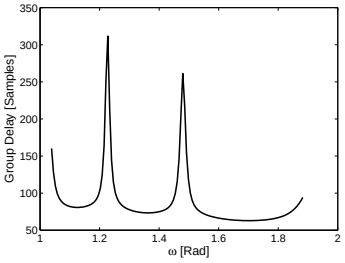

Figure 16. Group Delay Frequency-Response of the Overall CSD Bandpass FRM IIR Digital Filter $H(e^{j\omega})$ Before PSO

Multiplier	CSD Representation	Decimal Value
$m_{C_{0,1}}$	$00001.000\bar{1}00\bar{1}$	0.9297
$m_{C_{0,2}}$	$00010.000\bar{1}0\bar{1}0$	1.9219
$m_{L_{0,2}}$	00000.1000010	0.5156
$m_{C_{1,1}}$	$00001.00\bar{1}00\bar{1}0$	0.8594
$m_{C_{1,2}}$	$10000.\bar{1}0\bar{1}0000$	15.375
$m_{L_{1,1}}$	$00001.000\bar{1}0\bar{1}0$	0.9219
$m_{L_{1,2}}$	$00000.0010\bar{1}0\bar{1}$	0.0859

Table 6. Digital Multiplier Values for the Lowpass Section of the Bandpass FRM IIR Digital Filter

Based on the infinite-precision bandpass FRM IIR digital filter, the corresponding CSD FRM IIR initial digital filter is obtained to have a magnitude and group delay frequency responses as shown in Figs. 15 and 16.

By applying the proposed PSO to the initial FRM IIR digital filter and after about 160 iterations, the PSO converges to the optimal bandpass FRM IIR digital filter having a magnitude frequency response as shown in Fig. 17. In addition, Fig. 18 gives us a closer look to the magnitude frequency response of the passband region of the bandpass FRM IIR digital filter. Fig. 19 illustrates the group delay frequency response of the optimized bandpass FRM IIR digital filter. The values of the multiplier coefficients for the lowpass and highpass sections of the bandpass FRM IIR digital filter are obtained as summarized in Tables 6 and 7.

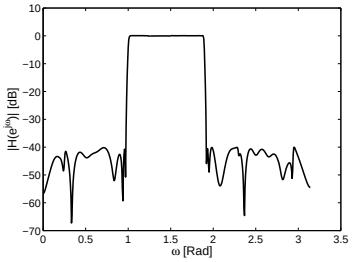

Figure 17. Magnitude Frequency-Response of the Overall CSD Bandpass FRM IIR Digital Filter $H(e^{j\omega})$ After PSO

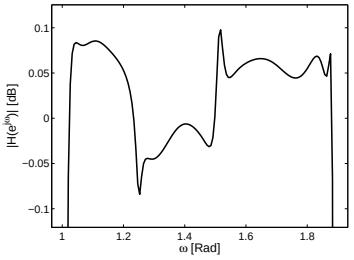

Figure 18. Magnitude Frequency-Response of the Passband Region of the Overall CSD Bandpass FRM IIR Digital Filter $H(e^{j\omega})$ After PSO

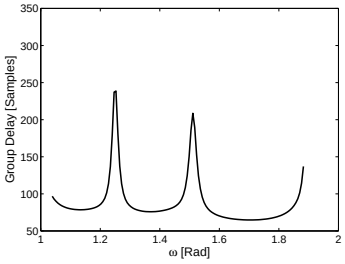

Figure 19. Group Delay Frequency-Response of the Overall CSD Bandpass FRM IIR Digital Filter $H(e^{j\omega})$ After PSO

Multiplier	CSD Representation	Decimal Value
$m_{C_{0,1}}$	$00001.00\bar{1}0\bar{1}00$	0.8438
$m_{C_{0,2}}$	$00010.0001001\bar{1}$	2.0547
$m_{L_{0,2}}$	$00000.1000001\bar{1}$	0.4922
$m_{C_{1,1}}$	$00001.0\bar{1}00010$	0.7656
$m_{C_{1,2}}$	10000.0100001	16.2578
$m_{L_{1,1}}$	$00001.0000\bar{1}01$	0.9766
$m_{L_{1,2}}$	$00000.0010\bar{1}0\bar{1}$	0.0859

Table 7. Digital Multiplier Values for the Highpass Section of the Bandpass FRM IIR Digital Filter

Frequency-Response Characteristic	Before PSO	After PSO
Maximum Passband Ripple A_p	0.8982[dB]	0.0978[dB]
Minimum Stopband Loss A_a	9.1715[dB]	40.0172[dB]
Maximum Group Delay	312[Samples]	239[Samples]

Table 8. Frequency-Response Analysis of the CSD Bandpass FRM IIR Digital Filter Before and After PSO

Table 8 represents the comparison of the CSD bandpass FRM IIR digital filters before and after PSO.

http://dx.doi.org/10.5772/52196

Author details

Seyyed Ali Hashemi and Behrouz Nowrouzian

Department of Electrical and Computer Engineering, University of Alberta, Edmonton, Alberta, Canada

References

[1] D. R. Wilson, D. R. Corrall, and R. F. Mathias, "The Design and Application of Digital Filters," *IEEE Transactions on Industrial Electronics and Control Instrumentation*, vol. IECI-20, pp. 68–74, 1973.

[2] P. P. Vaidyanathan, "Multirate digital filters, filter banks, polyphase networks, and applications: a tutorial," *Proceedings of the IEEE*, vol. 78, pp. 56–93, 1990.

[3] Y. C. Lim, "Frequency-Response Masking Approach for the Synthesis of Sharp Linear Phase Digital Filters," *IEEE Transactions on Circuits and Systems*, vol. 33, no. 4, pp. 357–364, 1986.

[4] ——, "A Digital Filter Bank for Digital Audio Systems," *IEEE Transactions on Circuits and Systems*, vol. 33-8, p. 848 âĂŞ 849, Aug. 1986.

[5] Y. C. Lim, S. R. Parker, and A. G. Constantinides, "Finite Word Length FIR Filter Design Using Integer Programming over a Discrete Coefficient Space," *IEEE Transactions on Acoustics, Speech and Signal Processing*, vol. 30, pp. 661–664, 1982.

[6] T. Saramaki and Y. C. Lim, "Use of the Remez Algorithm for Designing FIR Filters Utilizing the Frequency-Response Masking Approach," in *1999 IEEE International Symposium on Circuits and Systems. ISCAS '99*, vol. 3, 1999, pp. 449–455.

[7] Y. J. Yu and Y. C. Lim, "FRM Based FIR Filter Design - the WLS Approach," in *2002 IEEE International Symposium on Circuits and Systems. ISCAS 2002*, vol. 3, 2002, pp. III–221 – III–224.

[8] W.-S. Lu and T. Hinamoto, "Optimal Design of Frequency-Response-Masking Filters Using Semidefinite Programming," *IEEE Transactions on Circuits and Systems I: Fundamental Theory and Applications*, vol. 50, pp. 557–568, 2003.

[9] ——, "Optimal Design of FIR Frequency-Response-Masking Filters Using Second-Order Cone Programming," in *Proceedings of 2003 IEEE International Symposium on Circuits and Systems. ISCAS '03*, vol. 3, 2003, pp. III–878 – III–881.

[10] L. Cen and Y. Lian, "Hybrid Genetic Algorithm for the Design of Modified Frequency-Response Masking Filters in a Discrete Space," *Circuits, Systems, and Signal Processing*, vol. 25, pp. 153–174, April 2006.

[11] S. Chen, R. H. Istepanian, and B. L. Luk, "Digital IIR Filter Design Using Adaptive Simulated Annealing," *Digital Signal Processing*, vol. 11, no. 3, pp. 241–251, July 2001.

[12] K. sang Tang, K. fung Man, S. Kwong, and Z. feng Liu, "Design and Optimization of IIR Filter Structure Using Hierarchical Genetic Algorithms," *IEEE Transactions on Industrial Electronics*, vol. 45, no. 3, pp. 481–487, 1998.

[13] C. Dai, W. Chen, and Y. Zhu, "Seeker Optimization Algorithm for Digital IIR Filter Design," *IEEE Transactions on Industrial Electronics*, vol. 57, no. 5, pp. 1710–1718, May 2010.

[14] M. Najjarzadeh and A. Ayatollahi, "FIR Digital Filters Design: Particle Swarm Optimization Utilizing LMS and Minimax Strategies," in *IEEE International Symposium on Signal Processing and Information Technology, 2008. ISSPIT 2008.*, 2008, pp. 129–132.

[15] C. Dai, W. Chen, Y. Zhu, and X. Zhang, "Seeker Optimization Algorithm for Optimal Reactive Power Dispatch," *IEEE Transactions on Power Systems*, vol. 24, no. 3, pp. 1218–1231, August 2009.

[16] A. Kalinli and N. Karaboga, "A New Method for Adaptive IIR Filter Design Based on Tabu Search Algorithm," *AEU - International Journal of Electronics and Communications*, vol. 59, no. 3, pp. 111–117, May 2005.

[17] N. Karaboga, A. Kalinli, and D. Karaboga, "Designing Digital IIR Filters Using Ant Colony Optimisation Algorithm," *Engineering Applications of Artificial Intelligence*, vol. 17, no. 3, pp. 301–309, April 2004.

[18] A. Kalinli and N. Karaboga, "Artificial Immune Algorithm for IIR Filter Design," *Engineering Applications of Artificial Intelligence*, vol. 18, no. 5, pp. 919–929, Dec 2005.

[19] R. Storn, "Designing Nonstandard Filters with Differential Evolution," *IEEE Signal Processing Magazine*, vol. 22, no. 1, pp. 103–106, Jan 2005.

[20] N. Karaboga, "Digital IIR Filter Design Using Differential Evolution Algorithm," *EURASIP Journal on Applied Signal Processing*, vol. 2005, no. 8, pp. 1269–1276, Jan 2005.

[21] P. Mercier, S. M. Kilambi, and B. Nowrouzian, "Optimization of FRM FIR Digital Filters Over CSD and CDBNS Multiplier Coefficient Spaces Employing a Novel Genetic Algorithm," *Journal of Computers*, vol. 2, no. 7, pp. 20–31, Sept. 2007.

[22] S. Bokhari and B. Nowrouzian, "DCGA Optimization of Lowpass FRM IIR Digital Filters Over CSD Multiplier Coefficient Space," in *52nd IEEE International Midwest Symposium on Circuits and Systems*, August 2009, pp. 573–576.

[23] S. Bokhari, B. Nowrouzian, and S. A. Hashemi, "A novel technique for DCGA optimization of guaranteed BIBO stable IIR-based FRM digital filters over the CSD multiplier coefficient space," in *proceedings of 2010 IEEE International Symposium on Circuits and Systems (ISCAS)*, 2010, pp. 2710–2713.

[24] S. A. Hashemi and B. Nowrouzian, "Particle swarm optimization of FRM FIR digital filters over the CSD multiplier coefficient space," in *proceedings of 53rd IEEE International Midwest Symposium on Circuits and Systems (MWSCAS)*, 2010, pp. 1246–1249.

[25] ——, "A novel discrete particle swarm optimization for FRM FIR digital filters," *Journal of Computers*, vol. 7, no. 7, July 2012.

http://dx.doi.org/10.5772/52196

[26] ——, "Discrete particle swarm optimization of magnitude response of iir-based frm digital filters," in *proceedings of 17th IEEE International Conference on Electronics, Circuits, and Systems, 2010. ICECS 2010.*, December 2010.

[27] ——, "A novel finite-wordlength particle swarm optimization technique for frm iir digital filters," in *proceedings of 2011 IEEE International Symposium on Circuits and Systems (ISCAS)*, May 2011, pp. 2745–2748.

[28] J. Kennedy and R. Eberhart, "Particle Swarm Optimization," in *Proceedings of IEEE International Conference on Neural Networks*, vol. 4, 1995, pp. 1942–1948.

[29] M. D. Lutovac and L. D. Milić, "IIR Filters Based on Frequency-Response Masking Approach," in *Telecommunications in Modern Satellite, Cable and Broadcasting Service, TELSIKS 2001*, Sept. 2001, pp. 163–170.

[30] H. Johansson and L. Wanhammar, "High-speed Recursive Filtering Using the Frequency-Response Masking Approach," in *Proceedings of the IEEE Int. Symposium on Circuits and Systems*, 1997, pp. 2208–2211.

[31] J. Sun, W. Fang, and W. Xu, "A Quantum-Behaved Particle Swarm Optimization With Diversity-Guided Mutation for the Design of Two-Dimensional IIR Digital Filters," *IEEE Transactions on Circuits and Systems II: Express Briefs*, vol. 57, no. 2, pp. 141–145, 2010.

[32] A. Slowik and M. Bialko, "Design and Optimization of IIR Digital Filters with Non-Standard Characteristics Using Particle Swarm Optimization Algorithm," in *14th IEEE International Conference on Electronics, Circuits and Systems, ICECS 2007*, 2007, pp. 162–165.

[33] B. Luitel and G. K. Venayagamoorthy, "Particle Swarm Optimization with Quantum Infusion for the design of digital filters," in *IEEE Swarm Intelligence Symposium, SIS 2008*, 2008, pp. 1–8.

[34] B. Nowrouzian and L. S. Lee, "Minimal Multiplier Realisation of Bilinear-LDI Digital Allpass Networks," in *IEE Proceedings on Devices and Systems, G Circuits*, vol. 136, Jun. 1989, pp. 114–117.

[35] T. Parks and J. McClellan, "Chebyshev Approximation for Nonrecursive Digital Filters with Linear Phase," *IEEE Transactions on Circuit Theory*, vol. CT-19, pp. 189–194, 1972.

[36] Y. C. Lim, R. Yang, D. Li, and J. Song, "Signed Power-of-Two Term Allocation Scheme for the Design of Digital Filters," *IEEE Transactions on Circuits and Systems II: Analog and Digital Signal Processing*, vol. 46, pp. 577–584, 1999.

[37] R. I. Hartley, "Subexpression Sharing in Filters Using Canonic Signed Digit Multipliers," *IEEE Transactions on Circuits and Systems II: Analog and Digital Signal Processing*, vol. 43, pp. 677–688, 1996.

[38] A. T. G. Fuller, B. Nowrouzian, and F. Ashrafzadeh, "Optimization of FIR Digital Filters over the Canonical Signed-Digit Coefficient Space Using Genetic Algorithms," in *1998 Midwest Symposium on Circuits and Systems*, 1998, pp. 456–459.

[39] R. Yang, Y. C. Lim, and S. R. Parker, "Design of sharp linear-phase FIR bandstop filters using the frequency-response-masking technique," *Circuits, Systems, and Signal Processing*, vol. 17, no. 1, pp. 1–27, Jan. 1998.

[40] A. Willson and H. Orchard, "Insights into Digital Filters Made as the Sum of Two Allpass Functions," *IEEE Trans. On Circuits And Syst.*, vol. 42, pp. 129–137, Mar. 1995.

[41] D. Rabrenovic and M. Lutovac, "Elliptic filters with minimal Q-factors," in *IEE Electronics Letters Online*, vol. 30, no. 3, Feb. 1994, pp. 206–207.

[42] L. D. Milić and M. D. Lutovac, "Design of Multiplierless Elliptic IIR Filters with a Small Quantization Error," *IEEE Transactions on Signal Processing*, vol. 47, no. 2, pp. 469–479, Feb. 1999.

[43] M. D. Lutovac and L. D. Milić, "Design of Computationally Efficient Elliptic IIR Filters with a Reduced Number of Shift-and-Add Operations in Multipliers," *IEEE Transactions on Signal Processing*, vol. 45, no. 7, pp. 2422–2430, Oct. 1997.

[44] B. Nowrouzian, "A Novel Approach to the Exact Design of LDI Symmetrical Digital and Switched-Capacitor Filters," in *Proceedings of 33rd Midwest Symposium on Circuits and Systems*, vol. 2, Aug. 1990, pp. 967–972.

[45] V. Valkenburg, *Introduction to Modern Network Synthesis*. John Wiley and Sons, Inc., 1965.

[46] F. van den Bergh and A. P. Engelbrecht, "A Cooperative Approach to Particle Swarm Optimization," *IEEE Transactions on Evolutionary Computation*, vol. 8, no. 3, pp. 225–239, 2004.

[47] A. Antoniou, *Digital Filters: Analysis, Design, and Applications*. McGraw Hill, Inc., 1993.

[48] R. E. Crochiere, "Digital Network Theory and its Application to the Analysis and Design of Digital Filters," Ph.D. dissertation, M.I.T, Dep. of Elec. Eng., M.I.T, Cambridge, MA, May 1974.